Rotational and vibrational spectroscopy of 1-cyanoadamantane and 1-isocyanoadamantane

Olivia Chitarra[a,*], Marie-Aline Martin-Drumel[a], Zachary Buchanan[b], Olivier Pirali[a,c]

[a] *Université Paris-Saclay, CNRS, Institut des Sciences Moléculaires d'Orsay, 91405 Orsay, France*
[b] *Department of Chemistry, The University of California Davis, Davis, CA, USA*
[c] *SOLEIL Synchrotron, AILES beamline, l'Orme des Merisiers, Saint-Aubin, 91190 Gif-sur-Yvette, France*

Abstract

Because of their high stability, the presence of diamond-type molecules has long been suspected in the interstellar medium, a hypothesis supported by the extraction of diamond nanocrystal from some meteorites. We report the rotational and vibrational investigation of two polar derivatives of adamantane ($C_{10}H_{16}$), 1-cyanoadamantane ($C_{10}H_{15}$−CN) and 1-isocyanoadamantane ($C_{10}H_{15}$−NC), using room temperature gas phase absorption spectroscopy. Pure rotational spectra have been recorded at millimeter wavelengths (75–220 GHz) while vibrational spectra were obtained in the far- and mid-infrared domains (50–3500 cm^{-1}). Quantum chemical calculations have been performed on these two C_{3v} rotors to support the spectral analysis enabling the assignment, for both species, of more than 7000 pure rotational transitions in the ground (A_1 symmetry) and first vibrationally excited (E symmetry) states, and of most of the infrared active bands. The pure rotational lines were fit to their experimental accuracy using a symmetric-top Hamiltonian. Our study provides all necessary information for an active search of these species in space.

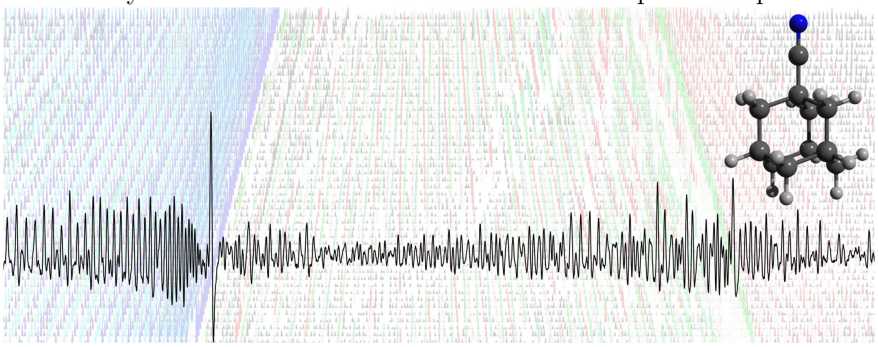

Keywords: Cyano-adamantanes, Rotational and vibrational spectroscopy, Astrophysical relevance

1. Introduction

Diamond-related materials relevance for a wide range of different research areas has motivated a great wealth of studies on these compounds since decades. Within this very large variety of materials, diamondoids possess tridimensional sp3 hybridized carbon cage structures terminated by hydrogen atoms conferring exceptional electronic, optical, and mechanical properties to these systems [1, 2, 3] which have received strong interest for various applications such as material science, biomedecine, nanotechnology, and environmental science (see, e.g., reviews on the synthesis and applications of diamondoids in Refs. [4, 5]). In the context of astrochemistry, these molecules have long been suspected to be present in various objects of the universe. Early 1969, based on the high stability of these samples and their resistance to UV photons, Saslaw and Gaustad [6] proposed diamond-like particles to be an important part of the gas and dust material present in space. This hypothesis was con-

*olivia.chitarra@universite-paris-saclay.fr

firmed in 1987 by Lewis et al. [7], who extracted nanometer sized diamond material from meteorites, and more recently by Jones et al. [8], who demonstrated the large abundance of these samples in primitive meteorites. In the interstellar medium, a striking agreement between the absorption spectra of synthetic nanodiamond thin films [9, 10] with the unusual emission bands located at 3.43 µm and 3.53 µm of few Herbig AeBe stars (in particular HD 97048 and Elias 1) has been reported by Guillois et al. [11]. To provide complementary insights into the size and structure of the proposed emitters, solid state as well as gas phase infrared (IR) spectroscopy were performed on pure diamondoids, at the molecular level, in the group of J. Oomens [12, 13]. These samples, ranging from adamantane ($C_{10}H_{16}$) to hexamantane ($C_{26}H_{30}$), were provided by the group of Carlson et al. who succeeded in isolating pure samples of large diamondoids using successive distillation processes in petroleum [14]. It is important to note that even though the chemical syntheses of adamantane and some of its derivatives are known since 1957 [15] and that several of these samples are commercially available nowadays, the laboratory synthesis of larger diamondoids only exists for diamantane (2 cages, $C_{14}H_{20}$) [16], triamantane (3 cages, $C_{18}H_{24}$) [17], tetramantane (4 cages, $C_{22}H_{28}$) [18], and pentamantane (5 cages, $C_{26}H_{32}$) [18]; the field thus remains very active in organic chemistry because of the exceptional properties of these materials [4]. The relatively recent access to pure molecular samples of large diamondoids from the Carlson group (up to undecamantane, 11 cages), opened the possibility to characterize their optical properties in the astrophysical context [19] and compare it to the infinite diamond lattice [20]. In addition to all these spectroscopic characterizations of the neutral molecules, laser-based IR multi-photon dissociation spectra were obtained for the dehydrogenated cationic forms of adamantane [21] as well as diamantane and triamantane [22].

Similarly to the well studied polycyclic aromatic hydrocarbons (PAHs) species, the smallest samples of the diamondoid family lack permanent dipole moment (the lightest diamondoid which exhibits a relatively small permanent dipole moment is tetramantane) preventing their searches in the interstellar medium using powerful radioastronomy observational platforms (e.g., GBT, NOEMA, ALMA). In the laboratory, rotational structure information on the smallest samples, e.g., the tetrahedral species adamantane and its N-substituted derivative hexamethylenetetramine ($C_6H_{12}N_4$), has been obtained using gas phase mid-IR and far-IR spectroscopy techniques. Spectra recorded at the SOLEIL synchrotron facility enabled the observation of the most intense IR-active bands in the 400–1500 cm^{-1} range [23, 24, 25] while the powerful technique of buffer gas cooling allowed the investigation of the congested 3 µm region in rotationally cold conditions [26]. The recent interstellar detections of several hydrocarbons containing a cyano functional group by the GOTHAM team, i.e., benzonitrile ($c-C_6H_5-CN$) [27, 28], cyanocyclopentadiene ($c-C_5H_5-CN$) [29], the cyanopolyyne $HC_{11}N$ [30], and cyanonaphthalenes ($C_{10}H_7-CN$ [29, 30]) open up the possibility of detecting other families of functionalized large C-bearing species possessing a strong permanent dipole moment.

In this context, we have investigated the rotational and vibrational absorption spectra of the 1-cyanoadamantane ($C_{10}H_{15}CN$, hereafter AdaCN) and 1-isocyanoadamantane ($C_{10}H_{15}NC$, hereafter AdaNC) molecules (Fig. 1). To our knowledge, a single high resolution spectroscopic investigations has been reported on these samples. Chadwick et al. [31] measured 4 transitions of AdaCN, with unresolved K structures, around 30 GHz allowing a first estimation of the B rotational constant in the ground and 3 vibrationally excited states. In the present work, the pure rotational spectra of AdaCN and AdaNC have been recorded at room temperature in the millimeter-wave region allowing the determination of accurate rotational constants in the ground and first excited vibrational states. In addition, we measured their gas-phase vibrational spectra in the 50–3500 cm^{-1} spectral range at room temperature and we performed quantum chemical calculations to support the analysis. The paper contains the experimental and computational details in section 2, the results and discussion are presented in section 3.

2. Laboratory methods

2.1. Samples

Samples of AdaCN (97 % purity) and AdaNC (95 % purity) were purchased from Sigma Aldrich and used without further purification.

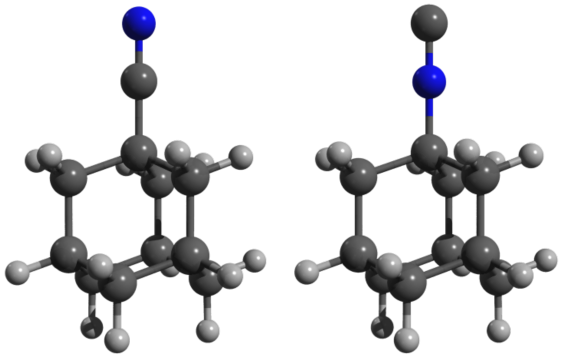

Figure 1: Molecular structure of the AdaCN (*left*) and AdaNC (*right*) molecules (the bond orders are not represented).

2.2. Infrared spectroscopy

The vibrational spectra of AdaCN and AdaNC have been recorded on the AILES beamline of SOLEIL synchrotron using a Fourier-transform interferometer (Bruker IFS 125) and a long absorption pathlength cell; an experimental set-up often employed to record absorption spectra of relatively large molecules (see for example Ref. [32]). In the mid-IR range (600–3000 cm^{-1}), the interferometer was equipped with a KBr beamsplitter together with a liquid-nitrogen cooled HgCdTe detector, and in the far-IR range (50–600 cm^{-1}) a 6 µm mylar composite beamsplitter and a liquid He cooled bolometer detector were used. The room temperature vapor pressure (a few µbar) of the samples was injected in the multi-pass cell allowing for 150 m absorption pathlength. The set of windows separating the absorption cell and the FT interferometer were made of ZnSe (0.5 ° wedged) when recording the mid-IR spectra and of 50 µm thick polypropylene films when recording the far-IR spectra.

The black upper traces of Fig. 2 show the absorption spectra of both AdaCN and AdaNC recorded in the far-IR and mid-IR spectral ranges, respectively. The spectra consist of the co-addition of 500 scans recorded with a spectral resolution of 1 cm^{-1}. Because the vibrational bands are broad, yielding rotationally unresolved features, we estimate the accuracy of the band positions to be a few cm^{-1} in average for all the bands. Attempts to resolve the rotational structure of the far-IR bands have been undertaken using the synchrotron radiation extracted by the AILES beamline and the highest spectral resolution of the FT interferometer (about 30 MHz), without success. The high density of lines and the presence of numerous hot bands, involving several quanta of low frequency modes populated at room temperature, are causing significant spectral congestion.

2.3. Millimeter-wave spectroscopy

The rotational spectra of both molecules were recorded using an absorption set-up adapted to investigate the millimeter and sub-millimeter wave spectra of non reactive species [33]. The spectrometer consists of a radio-frequency synthesizer feeding a solid-state multiplication chains from Radiometer Physics GmbH (RPG) or Virginia Diode Inc. (VDI) covering the 75–950 GHz range. The absorption cell is a 2 m long, 50 mm inner diameter Pyrex tube equipped with Teflon windows at both ends. The spectra were recorded in the 75–220 GHz range, where the most intense absorption signals are expected at room temperature for both species. We used a frequency modulation scheme associated with a second harmonic phase sensitive lock-in detection. The modulation frequency was set to 48.157 kHz for all recordings. The modulation depth, the time constant, and the frequency steps depend on the spectral region studied, on the absorption signal, and on the line density of the spectrum. The vapor pressure of both samples (in the µbar range at room temperature) was injected in the cell using a constant slow flow of gas ensured by a turbomolecular pump. To record the absorption spectrum of AdaCN in the 75–110 GHz, we injected about 3.3 µbar of the sample in the cell; we chose a modulation depth corresponding to 130 kHz, a time constant of 100 ms, and a frequency step of 30 kHz. In the 140–220 GHz range, the pressure was 1.7 µbar, the frequency depth was set to 260 kHz, the time constant was 20 ms, and the frequency step was 30 kHz. For the 75–110 GHz spectrum of AdaNC, the pressure was 1.7 µbar, the frequency depth was 130 kHz, the frequency step was set to 30 kHz, the time constant was 100 ms. Finally, we used a 260 kHz frequency depth, 50 kHz frequency step, and 50 ms time constant to record the AdaNC spectrum in the 140–220 GHz range. The line position accuracy is estimated based on the signal-to-noise ratio of the transitions: for AdaCN a unique value of 30 kHz is used over the whole spectral range while for AdaNC 30 kHz and 50 kHz are used in the 75–110 GHz and 140–220 GHz ranges, respectively.

The black traces of Fig. 3 show a portion of the pure rotation spectrum of AdaCN recorded in

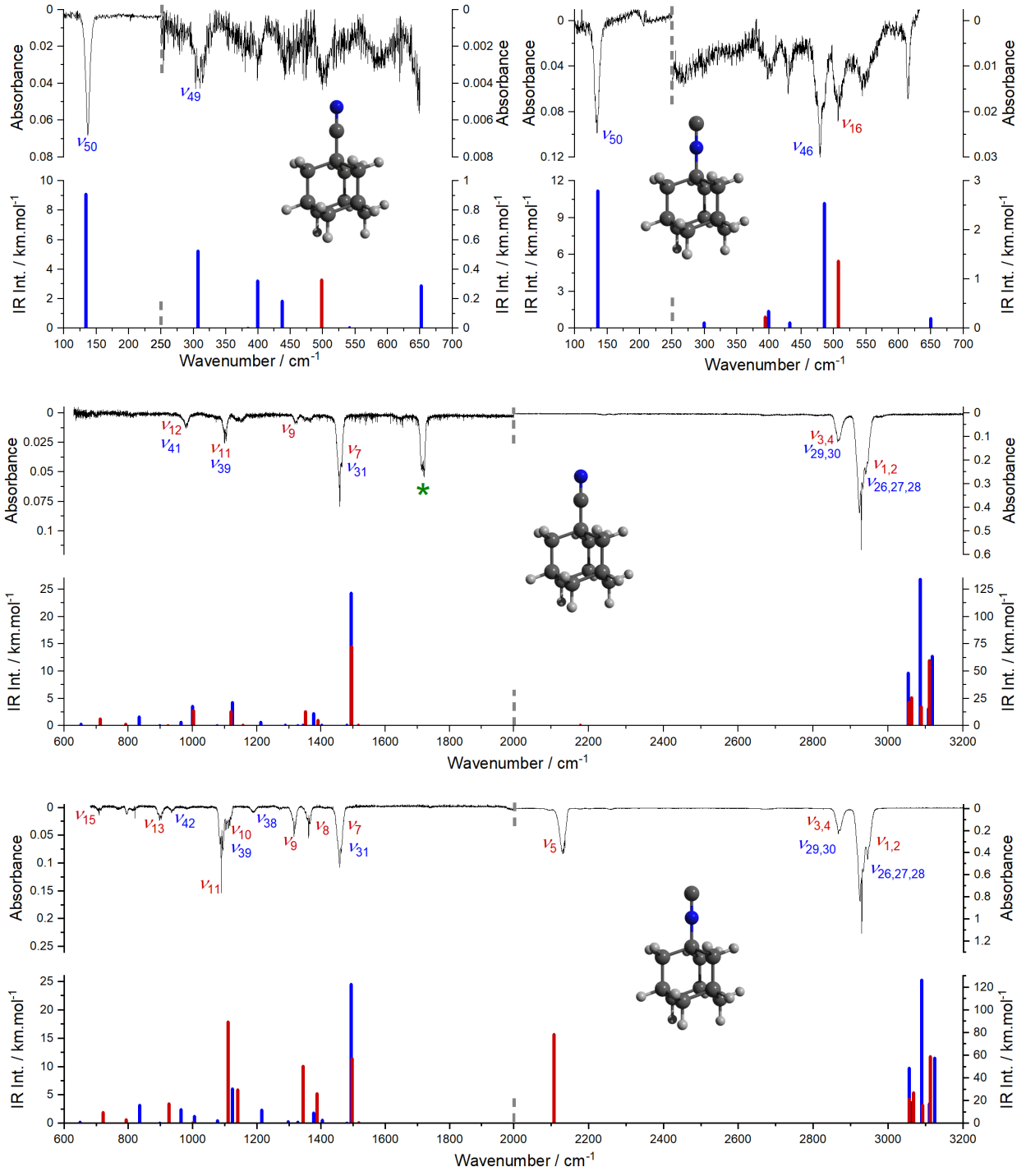

Figure 2: Far-IR (top traces) and mid-IR (middle and bottom traces) of AdaCN (top left and middle) and AdaNC (top right and bottom) recorded using the FT-IR interferometer of the AILES beamline at SOLEIL. Black traces correspond to the experimental absorbance spectra and stick plots correspond to calculated band positions at the MP2/cc-pVTZ level of theory. Vibrational bands of E symmetry are represented in blue, and those of A_1 symmetry in red. Note the different intensity scale for the lower and upper frequency region of each spectrum (split at 250 cm^{-1} in the far-IR and 2000 cm^{-1} in the mid-IR). The band identified by an asterisk in the mid-IR spectrum of AdaCN (middle panel) arises from an impurity containing a carbonyl group.

our work. The left part of the figure shows a portion recorded in the 166.5–171 GHz region, where 3 dense clusters of a-type transitions involving the ground vibrational state (GS) as well as few excited states (ES) populated at room temperature can be clearly observed. The right part of the figure gives a zoom into one K ladder involving GS pure rotation transitions with $J' = 99$.

2.4. Quantum chemical calculations

In order to support the analysis of the rotational and vibrational spectra of AdaCN and AdaNC, we performed quantum chemical calculations using the Gaussian09 software [34]. Geometry optimization as well as the energies of vibrational states in the harmonic approximation were calculated using MP2 method and cc-pVTZ basis set [35]. The optimized equilibrium structures are reported in the supplementary material and represented on Fig. 1.

3. Results and discussion

3.1. Spectroscopic considerations

Both AdaCN and AdaNC molecules belong to the C_{3v} group of symmetry and possess a $^1A_1$ electronic ground state, 75 vibrational degrees of freedom, and 50 vibrational modes. The irreducible representation for the vibrational modes is:

$$\Gamma = 17\ \mathrm{A}_1 \oplus 8\ \mathrm{A}_2 \oplus 25\ \mathrm{E} \tag{1}$$

The A_1 and E vibrational bands are labeled parallel and perpendicular bands, respectively. Those of A_2 symmetry are IR inactive. Concerning the rotational structure of the molecules, both species are symmetric tops with calculated permanent dipole moments along the a axis of symmetry of 4.9 Debye for AdaCN and 4.2 Debye for AdaNC. We used the conventional equation to calculate the energy levels of both molecules in their GS and ES [36] as implemented in the Pickett's CALPGM software:

$$\begin{aligned} E_v(J,K,l) =& B_v J(J+1) + (A_v - B_v)K^2 \\ &- D_{J_v} J^2(J+1)^2 - D_{JK_v} J(J+1)K^2 \\ &- D_{K_v} K^4 \\ &- 2A_v K l\zeta + 2[(2D_{J_v} + D_{JK_v})J(J+1) \\ &+ (2D_{K_v} + D_{JK_v})K^2]Kl\zeta + P(J,K,l) \\ &+ ... \end{aligned} \tag{2}$$

with :

$$P(J,K,l) = \pm \frac{[J(J+1) - K(K \mp 1)]}{8(K \mp 1)} \tag{3}$$

$$\times \frac{[J(J+1) - (K \mp 1)(K \mp 2)]}{[(1-\zeta)A_v - B_v]} q^2 \tag{4}$$

where :

$$q \approx \frac{2B_v^2}{\omega} \tag{5}$$

In equations (3)–(5), J and K are the rotational quantum numbers; A and B the rotational constants; D_J, D_{JK}, and D_K the centrifugal distortion constants; v denotes the vibrational state. For singly degenerated states of A_1 symmetry, $\zeta = 0$ and $P(J,K,l) = 0$. For E degenerated vibrational states (e.g., $v_{50} = 1$ in our study), the q parameter is the l-type doubling parameter, ζ is the Coriolis coupling constant, and ω is the fundamental vibrational frequency of the considered E state.

3.2. Assignment of the vibrational spectra

Figure 2 contains panels corresponding to the spectra recorded in the far-IR (upper panels) and mid-IR (middle and lower panels) of AdaCN and AdaNC, plotted in absorbance. At the spectral resolution used, the rotational contour (P-, Q-, R-branches) is distinguishable for some of the bands. Below the experimental spectra (black traces), we plotted the calculated positions and intensities of fundamental parallel bands (involving upper states of A_1 symmetry) in red, and perpendicular bands (involving upper states of E symmetry) in blue. We initially performed a simulation of the rotational contour of these calculated bands using the PGOPHER software [37], but many Q-branches of simulated parallel bands showed largely overestimated intensities (most likely because the same rotational constants were used for the upper and lower states) which complicated the assignment procedure rather than supported it. We preferred comparing the experimental trace with simple vertical bars corresponding to the frequencies and intensities of the calculated vibrational bands, directly available from the output files of Gaussian. Using this graphical comparison, we report in table 1 the proposed band assignments of the IR spectra for both molecules.

At first sight, the vibrational spectra of both AdaCN and AdaNC are very similar to the parent adamantane molecule and higher diamondoid

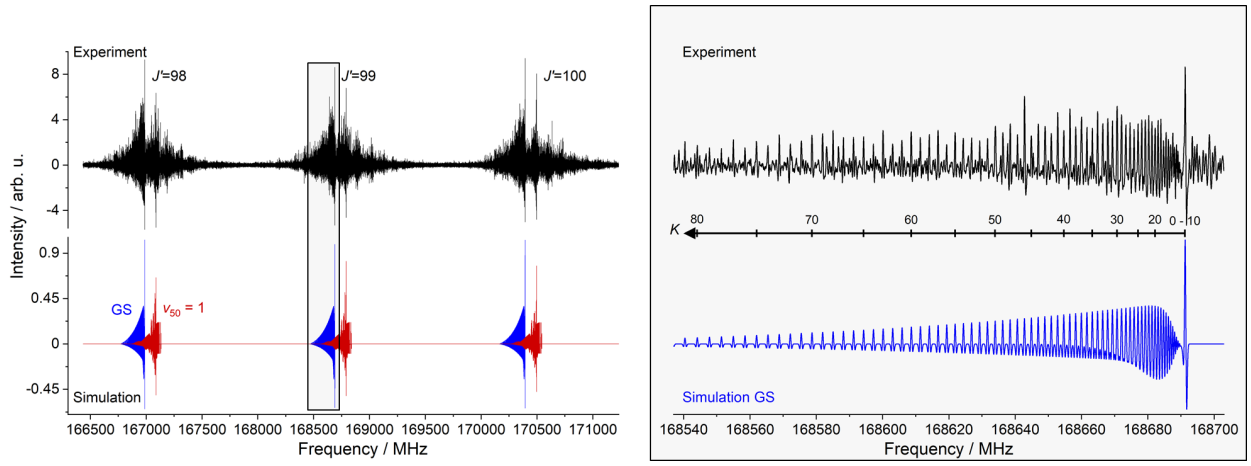

Figure 3: *Left:* 5 GHz portion of the millimeter-wave spectrum of AdaCN recorded in the 140–220 GHz spectral range displaying 3 clusters of a-type transitions involving $J' = 98$, $J' = 99$ and $J' = 100$ *Right:* Zoom onto one cluster of GS pure rotation transitions involving $J' = 99$. The black traces represent the experimental spectrum. The red and blue traces correspond to pure rotation transitions within the GS and $v_{50} = 1$, respectively, simulated using the final set of parameters (see the discussion). To enable visual comparison with the experimental trace, the plotted simulations correspond to the second derivative of the traces obtained with the PGOPHER software a full width at half maximum of 250 kHz (gaussian shape).

species [12]. For both species, several intense (more than 100 km/mol) CH stretching modes absorb in the 3000 cm^{-1} region leading to two distinct features located around 2860 cm^{-1} and 2930 cm^{-1} and dominating the IR spectrum. All other bands appear much weaker (few km/mol) with the exception of the scissoring mode bands located at about 1500 cm^{-1} (ν_7 and ν_{31}) with calculated intensities of about 20 km/mol for both species. In the case of AdaNC, an additional intense band corresponding to the CCN asymmetric stretching mode (ν_5) is calculated at 2108 cm^{-1} with an intensity of 78 km/mol. It is assigned to the 2133 cm^{-1} feature in the experimental spectrum with good confidence. In the case of AdaCN, the equivalent asymmetric stretching mode appears very weak both in the calculated and experimental spectra, but an intense feature is detected at about 1718 cm^{-1} and has no counterparts in the calculated spectrum. Because of its location and intensity, this band most likely arises from a contaminant containing a carbonyl group. The vibrational bands associated to CO stretching modes are extremely intense and a band at a similar energy (1740 cm^{-1}) has been observed for the CO stretching mode of 1-aza-adamantan-4-one ($C_9H_{13}NO$) [33] which was the most intense feature of its IR spectrum. In the hypothesis that the 1718 cm^{-1} feature arises from a molecule similar to adamantanone ($C_{10}H_{14}O$), its vibrational spectrum certainly affects other spectral regions of the AdaCN spectrum, in particular the CH stretching mode regions. We were not able to identify unambiguously any additional vibrational bands to guide our search for the nature of the impurity present in our sample.

Beside the relatively intense bands discussed above, the mid-IR experimental spectra exhibit several weaker bands located between 900 and 1400 cm^{-1}. The comparison with the calculated spectra allows us to propose assignments for some of these features (Table 1).

The far-IR spectra of both molecules (see the upper panel of figure 2) exhibit weak absorption bands corresponding mostly to deformations of the carbon cages. The calculated spectra are in good agreement with our experimental recordings and allow us to propose several relatively secure assignments. Note that for both AdaCN and AdaNC, the lowest frequency mode located around 135 cm^{-1} is assigned to a wagging of the CN group with respect to the rest of the carbon cage (ν_{50}). They are actually the most intense bands observed in the far-IR region (with calculated intensities of about 10 km/mol).

In absence of anharmonic calculations, the Calc./Exp. values can be compared with scaling factors commonly used in the literature [see, e.g., Ref. 12]. For both species, in the CH stretching region we obtain an average ratio of 0.94 while in the mid-IR range (500–2200 cm^{-1}) an average ratio of 0.98 is found. These values are in very good

agreement with the expected scaling factor of 0.95 recommended by the NIST for MP2/cc-pVTZ harmonic calculations [38].

3.3. Assignment of the rotational spectra

As in previous studies concerning the spectroscopy of relatively large C-bearing species, the high density of lines complicates the assignment of the pure rotation spectra. However, the combined use of different programs facilitated and secured the analysis. Our 3-steps assignment procedure is described in the following. (i) Using the results of the quantum chemical calculations and the PGOPHER software [37], we were able to simulate the ground state pure rotational spectra at 300 K and compare the calculated transitions with the experimental traces. A very rough fit of successive clusters of a-type transitions in PGOPHER provides a good estimation of the B_0 rotational constant which can then be inserted in a parameter file for the SPFIT/SPCAT suite of programs [39]. (ii) The calculated energy levels are then used by the LWW program for symmetric tops [40], creating Loomis-Wood plots hence providing a very convenient graphical support to search for branches involving the same K values and increasing values of J. (iii) Finally, all assigned branches are fit using the SPFIT program. Step (ii) and (iii) are performed as an iterative process. This approach has proven to be very efficient when dealing with highly congested spectra involving pure rotation or rotation-vibration transitions.

In the present study, as shown on the right panel of Fig. 3, the K-ladder assignment is not straightforward. Indeed, for low values of K, the high density of lines in a J cluster prevents at first an unambiguous assignment. However, with increasing K values, lines separated by one quantum of K are very well resolved. Therefore, to provide a secure assignment of the K-ladders, we used the LWW software to rapidly assign several tens of branches involving successive values of K and containing values of J typically ranging from $J = K$ up to $J = 100$. The definitive assignment of K was provided by performing fits in SPFIT while the values of K is incremented in all assigned branches. For this part of the analysis, we typically used a subset of more than 50 successive branches to perform the trials fits, and only the B and centrifugal distortion parameters were included in the model. Fig. 4 shows the results of this procedure for the assignment of the GS transitions of the AdaNC molecule. In this case, we used a subset of 68 successive branches (for a total of 3455 lines) to perform the fits. The upper plot of Fig. 4 provides the results of the fit for our initial guess assignment (represented as "shift of $K = 0$", RMS=73.5 kHz) as well as all results corresponding to shifts of the K values in all branches by $\pm 1, 2, 3, 4$. It is clear that the best fit is obtained when all values of K are shifted by -1 (RMS=41.7 kHz) from the initial assignment. A final confirmation of the K-ladder assignment is obtained by inputting the fitted rotational parameters in PGOPHER. An example of this comparison between the experimental spectrum of AdaNC and 3 simulated spectra produced from the different sets of constants is given on Fig. 4. On the figure, it is clear that while most of isolated lines seem to be well predicted in the simulation, the head of the K-ladder is clearly shifted when changing the assignment of K by one quantum. In this particular case, the initial assignment predicts the position of the band head at lower frequency (few hundreds of kHz) than the experiment. Subtracting one quantum from all values of K in every branch nicely reproduces the position of the band head, confirming the results of the fit. Both the standard deviation and the comparison of the band heads in PGOPHER confirmed our assignments.

Using the assignment procedure described above, we could relatively rapidly perform the assignment and fit of both AdaCN and AdaNC molecules in their vibrational ground state (which possesses A_1 symmetry). The list of fitted GS parameters is given in Table 2 for AdaCN and Table 3 for AdaNC. In the case of AdaCN, 4929 transitions were assigned in $v = 0$ involving K'' values from 0 to 119 and J'' up to 128; and 4375 transitions were assigned in $v_{50} = 1$ with similar J'' and $K'' \leq 91$ values. For AdaNC, 3968 and 3703 lines were assigned in $v = 0$ and $v_{50} = 1$, respectively, with $K'' \leq 91$ and $J'' \leq 123$. In both cases, the present experimental dataset allowed us to accurately fit B, D_J, D_{JK}, and the sextic H_{JK} and H_{KJ} terms (which were added to the model to include branches involving high values of J and K). Because only a-type transitions are observed, the A and D_K constants are kept fixed to the value derived from the equilibrium calculation. The standard deviation of each fit is close to 1.

The agreement between the calculated (equilibrium) and experimental (ground state) values for B is very good (less than 1 % relative differ-

Table 1: Vibrational modes of AdaCN and AdaNC calculated at the MP2/cc-pVTZ level and comparison with experimental assignments. Experimental bands are separated into two columns: confident assignments are presented in the column "Assign." and tentative ones in the column "Prop.". No scaling factor has been used in the calculated frequencies columns.

	AdaCN					**AdaNC**				
ν	Calculated [a]		Experimental			Calculated [a]		Experimental		
	Freq.	Int. [b]	Assign.	Prop.	δ [c]	Freq.	Int. [b]	Assign.	Prop.	δ [c]
Symmetry A_1										
1	3110	59.5	2927		-5.9	3113	58.7	2928		-5.9
2	3088	17.3	2927		-5.2	3091	27.0	2928		-5.3
3	3062	25.7	2866		-6.4	3067	21.4	2869		-6.5
4	3054	21.2	2866		-6.2	3056	21.4	2869		-6.1
5	2179	0.7		2254	3.4	2108	78.1	2133		1.2
6	1517	0.1				1518	0.1			
7	1495	14.5	1458		-2.5	1496	11.4	1459		-2.5
8	1391	1.0		1358	-2.4	1388	5.2	1361		-2.0
9	1352	2.6		1320	-2.4	1345	10.1	1316		-2.1
10	1157	0.2				1141	5.9	1111		-2.6
11	1120	2.6	1099		-1.8	1110	17.8	1089		-1.9
12	1003	2.8	979		-2.4	1001	0.1			
13	924	0.1				927	3.4	900		-2.9
14	791	0.3				793	0.6			
15	712	1.2		700	-1.7	722	1.9	709		-1.8
16	498	0.3		501	0.6	507	1.4	507		0.0
17	384	0.01				393	0.2		400	1.6
Symmetry E										
26	3118	63.7	2927		-6.1	3125	57.5	2928		-6.3
27	3107	15.7	2927		-5.8	3109	17.0	2928		-5.8
28	3086	134.1	2927		-5.2	3089	126.1	2928		-5.2
29	3060	21.4	2866		-6.3	3064	18.3	2869		-6.4
30	3054	48.3	2866		-6.2	3056	48.6	2869		-6.1
31	1493	24.3	1458		-2.3	1493	24.5	1459		-2.3
32	1480	0.1				1481	0.04			
33	1403	0.1				1404	0.5			
34	1378	2.2		1358	-1.4	1378	1.8			
35	1345	0.1				1345	0.9			
36	1328	0.04				1328	0.2			
37	1288	0.1				1298	0.3			
38	1212	0.69				1215	2.3	1189		-2.1
39	1124	4.2	1104		-1.8	1124	6.0	1111		-1.2
40	1077	0.007				1078	0.5			
41	1000	3.6	979		-2.1	1006	1.2			
42	963	0.6				964	2.4	936		-3.0
43	898	0.03				899	0.003			
44	834	1.6				835	3.1		793	-5.1
45	652	0.3				650	0.2		614	-5.5
46	541	0.003				486	2.5	478		-1.6
47	437	0.2		442	1.1	432	0.1			
48	399	0.3		397	-0.6	399	0.3		400	0.3
49	307	0.5	309		0.5	300	0.1			
50	134	9.1	137		2.4	135	11.2	134		-1.0

[a] Positions (Freq., $\tilde{\nu}$) are given in cm^{-1} and intensities in km/mol. [b] For vibrational bands with an E symmetry, the reported intensity corresponds to the sum of the two equivalent band intensities calculated by Gaussian [c] In % using $\delta = (\tilde{\nu}_{\text{exp.}} - \tilde{\nu}_{\text{calc.}})/\tilde{\nu}_{\text{calc.}} \times 100$

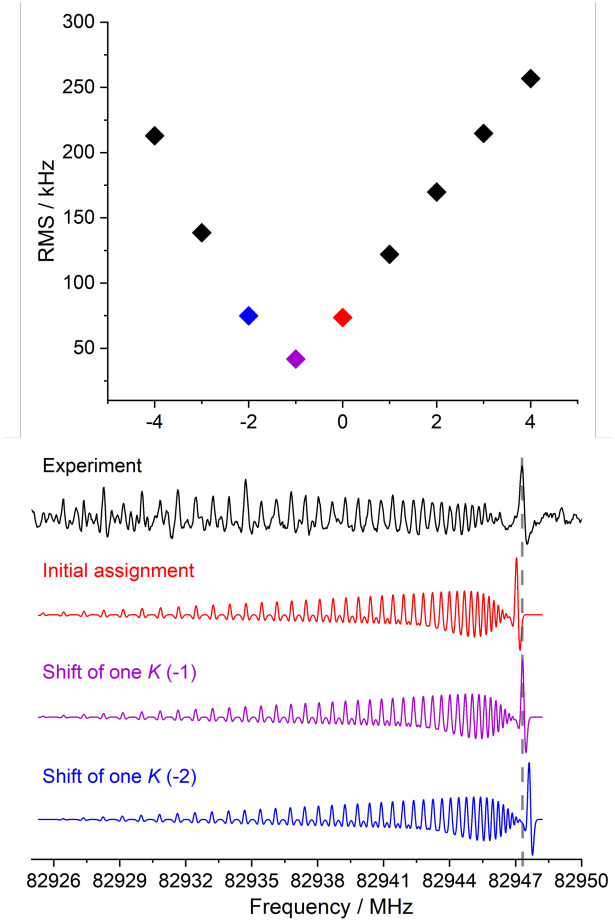

Figure 4: *Upper panel*: Results of different fits of AdaNC involving 68 successive branches plotted against incremented values of K in all assigned branches. The value 0 is our initial guess of K assignment. The lowest value of the RMS (about 42 kHz) indicates unambiguously the definitive assignment of the K ladders which is shifted by -1 from our initial guess. *Lower panel*: Comparison of the experimental spectrum (black trace) with 3 simulated spectra obtained by fitting the line list of GS transitions of AdaNC and applying a shift of -1, and -2 to K in all assigned branches. We clearly see the effect of misassignment of the K ladder by one quantum on the band head.

ence for both molecules). D_J shows a similarly good agreement while D_{JK} has similar values for both molecules but the calculations gave a slightly lower value, leading to a larger discrepancy between observed and calculated parameters for AdaCN. Like adamantane and its derivatives, AdaCN and AdaNC are rigid rotors as reflected by the small values of their centrifugal distortion constants (about 6 orders of magnitude smaller than B).

In addition to the pure rotation in the GS, we assigned pure rotation transitions within the first vibrationally excited state (ES), $v_{50} = 1$ (doubly degenerated state of E symmetry). For both AdaCN and AdaNC, $v_{50} = 1$ lies around 130 cm^{-1} above GS, which correspond to about 50 % of the ground state population at room temperature. In the ES, the structure of the a-type transitions clusters differs from the GS because of l-type doubling. Fig. 5 displays a small portion of the rotational absorption spectrum of AdaNC, showing a frequency span of 150 MHz around a cluster of GS lines in the 102 GHz spectral region (left part of the figure). A zoom into the cluster of lines involving $v_{50} = 1$ is shown on the right panel of Fig. 5. The splitting between $l = 1$ and $l = -1$ components is well resolved in our spectrum showing line progressions starting a few MHz higher in frequency for the $l = -1$ components. Using an estimated value of $q = 0.36$ MHz for AdaCN and 0.39 MHz for AdaNC (equation 5), we could repeat the GS assignment procedure, using independent Loomis-Wood diagrams for $l = 1$ and $l = -1$. As the lines involving $K = 0$ for $l = -1$ appear isolated, we started the analysis of successive branches rapidly and checked the K assignment, similar to what was done for the GS, by incrementing all values of K in the dataset and finding the lowest standard deviation of the fit. For branches involving $l = 1$, the assignment of the K structure was more complicated due to the branch head involving a multitude of small values of K (e.g., between 7 and 14 for AdaNC, see Fig. 5). As a consequence of the large number of potential assignments, our initial guess for assigning the K values was off by 10 quanta but fitting together $l = 1$ and $l = -1$ allowed us to rapidly find an unambiguous assignment. The results of the fit for the ES dataset are quite similar to the GS in terms of number of assigned transitions and values of J and K included in the fit. The fits, presented in tables 2 and 3, are very satisfactory, both rotational constants and l-doubling parameters being well determined.

Many unassigned lines grouped in clusters very similar to those assigned but with weaker intensity are present in the experimental spectra of both AdaCN and AdaNC. These lines most likely involve higher vibrational states populated at room temperature. We clearly see on Figure 3 a progression of hot bands involving higher quanta of v_{50}. Despite significant efforts to find a satisfactory analysis for $v_{50} = 2$, we were not able to provide any definitive assignment for the K ladders. One possi-

Table 2: Rotational constants of the ground state and the first excited state of AdaCN. Comparison of the fit with calculations. Values are in MHz unless otherwise noted.

	Eq.	GS		v_{50}=1 (ES)
	Calc.[a]	Exp.	δ[b]	Exp.
Rotational constants				
A	1698.76	[1698.76][c]		[1698.76][c]
B	858.47	852.218045 (11)	−0.73	852.771240 (13)
Centrifugal distortion constants				
$D_J \times 10^5$	1.22	1.231404 (47)	0.93	1.241490 (51)
$D_{JK} \times 10^4$	1.23	1.166870 (32)	−5.13	1.157348 (63)
$D_K \times 10^5$	−9.01	[−9.01][c]		[−9.01][c]
$H_{JK} \times 10^{11}$		4.443 (13)		4.068 (23)
$H_{KJ} \times 10^{11}$		−6.048 (18)		−5.811 (64)
***l*-doubling parameters**				
$-2A\zeta$				−2700.90 (35)
$\eta_J \times 10^3$				0.823705 (61)
q	0.36[d]			0.386501 (53)
Relevant fit parameters				
N[e]		4929		4375
$J''_{\max}$, $K''_{\max}$[f]		128,119		128,91
rms			0.033	
σ[g]			1.11	

[a] Calculated equilibrium value, MP2/cc-pVTZ, this work [b] in % using the formula $\delta = (B_{0\,\mathrm{exp.}} - B_{\mathrm{e\,calc.}})/B_{\mathrm{e\,calc.}} \times 100$ [c] Fixed to the calculated value [d] Calculated value of q in $v_{50} = 1$ [e] Number of assigned transitions [f] Unitless [g] Reduced standard deviation, unitless

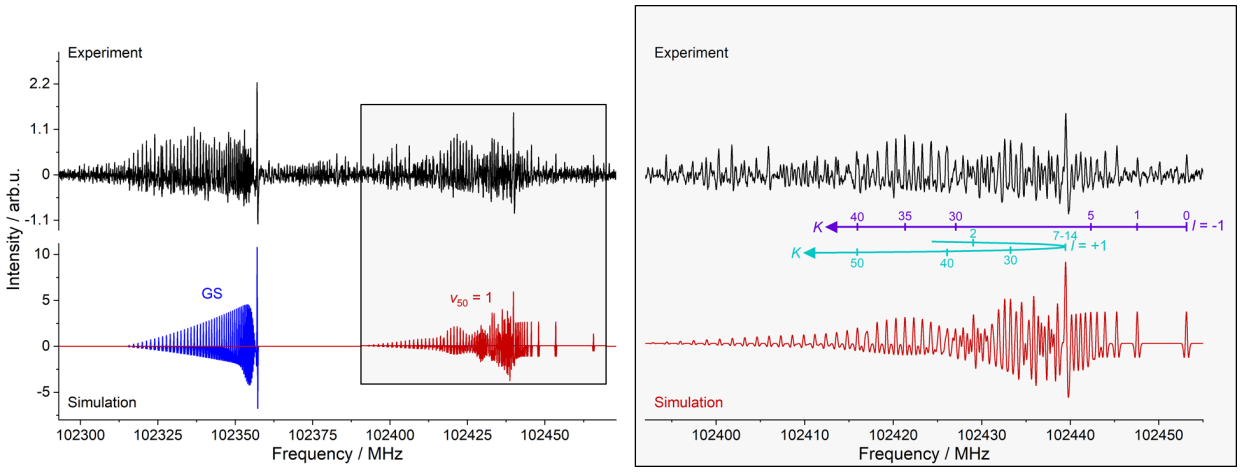

Figure 5: Portion of the pure rotation absorption spectrum of AdaNC showing a cluster of transitions involving $J'' = 57$. Black traces are the experimental spectrum, blue and red traces are simulated spectra in the ground and ν_{50} states, respectively, using the fitted parameters. The right panel shows a zoom of a typical cluster of pure rotation lines within the E symmetry ν_{50} state. As for the AdaCN plots displayed in Fig. 3, the simulations corresponds to the second derivative of the trace obtained using the PGOPHER software for the final set of rotation constants and a full width at half maximum of 250 kHz.

ble reason is that $v_{50} = 2$ falls in near coincidence with $v_{49} = 1$ (for which we did not succeed to per-

Table 3: Rotational constants of the ground state and the first excited state of AdaNC. Values are in MHz unless otherwise noted.

	Eq.	GS		v_{50}=1 (ES)
	Calc.[a]	Exp.	δ[b]	Exp.
Rotational constants				
A	1701.93	[1701.93][c]		[1701.93][c]
B	889.95	882.475497 (16)	−0.84	883.199299 (20)
Centrifugal distortion constants				
$D_J \times 10^5$	1.27	1.286431 (76)	1.29	1.301015 (92)
$D_{JK} \times 10^4$	1.10	1.099262 (81)	−0.07	1.08068 (13)
$D_K \times 10^5$	−7.78	[−7.78][c]		[−7.78][c]
$H_{JK} \times 10^{11}$		4.698 (30)		3.763 (43)
$H_{KJ} \times 10^{11}$		−6.834 (88)		−6.39 (23)
***l*-doubling parameters**				
$-2A\zeta$				−2850.2 (10)
$\eta_J \times 10^3$				1.11643 (12)
q	0.39[d]			0.41759 (14)
Relevant fit parameters				
N[e]		3968		3703
$J''_{\max}$, $K''_{\max}$[f]		123,91		123,77
rms			0.048	
σ[g]			1.01	

[a] Calculated equilibrium value, MP2/cc-pVTZ, this work [b] in % using the formula $\delta = (B_{0\,\mathrm{exp.}} - B_{\mathrm{e\,calc.}})/B_{\mathrm{e\,calc.}} \times 100$ [c] Fixed to the calculated value [d] Calculated value of q in $v_{50} = 1$ [e] Number of assigned transitions [f] Unitless [g] Reduced standard deviation, unitless

form any assignment either) and might be subject to some perturbations complicating even more the assignment of K branches. The fit files in Pickett's format (.lin, .par, .fit) are provided in the supporting information.

4. Conclusion

In this work, we provide a spectroscopic study of two cyano containing isomers of adamantane, AdaCN and AdaNC; both species belonging to the C_{3v} point group of symmetry. Both the vibrational (50–3000 cm^{-1}) and pure rotational (75–220 GHz) gas phase spectra of the two molecules were recorded at room temperature and their assignments were supported by quantum chemical calculations. Despite the relatively high density of rotational lines, the unambiguous analysis of the K structure for these heavy symmetric tops species was eased by careful investigation of the effect of successive K-values assignments on the RMS of the fit and typical spectral fingerprints. Accurate spectroscopic constants have been determined for both the GS and first ES ($v_{50} = 1$) of the two species.

Considering the large dipole moment of the two compounds, close to 4.5 Debye, these cyano-containing molecules appear as promising proxy for the centro-symmetric parent adamantane that possesses no pure rotational spectrum, similar to what has been seen for benzene using benzonitrile. Searches for AdaCN and AdaNC in the interstellar medium can now be undertaken with confidence using the reliable constants derived in this work.

Acknowledgement

This project received funding from the Région Ile-de-France, through DIM-ACAV$^+$, from the Programme National "Physique et Chimie du Milieu Interstellaire" (PCMI) of CNRS/INSU with INC/INP co-funded by CEA and CNES, from the "*Investissements d'Avenir*" LabEx PALM (ANR-10-LABX-0039-PALM), and from the *Agence Na-*

tionale de la Recherche (ANR-19-CE30-0017-01). The authors acknowledge the use of the computing center MésoLUM of the LUMAT research federation (FR LUMAT 2764). Z.S.B. acknowledges support from the Chateaubriand Fellowship of the Office for Science & Technology of the Embassy of France in the United States.

Appendix: Supplementary data

Supplementary data associated with this article (parameter and fit files) are available on ScienceDirect (www.sciencedirect.com).

Author contributions

Olivia Chitarra: Investigation, Formal analysis, Visualization, Writing – review & editing; Zachary Buchanan: Investigation, Writing – review & editing; Marie-Aline Martin-Drumel: Funding acquisition, Investigation, Supervision, Validation, Writing – review & editing; Olivier Pirali: Funding acquisition, Investigation, Supervision, Project administration, Validation, Writing – original draft;

References

[1] T. Demján, M. Vörös, M. Palummo, A. Gali, Electronic and optical properties of pure and modified diamondoids studied by many-body perturbation theory and time-dependent density functional theory, J. Chem. Phys. 141 (2014) 064308. doi:10.1063/1.4891930.

[2] L. Landt, K. Klünder, J. E. Dahl, R. M. K. Carlson, T. Möller, C. Bostedt, Optical response of diamond nanocrystals as a function of particle size, shape, and symmetry, Phys. Rev. Lett. 103 (2009) 047402. doi:10.1103/PhysRevLett.103.047402.

[3] G. A. Mansoori, Diamondoid molecules, in: Rice, SA (Ed.), Advances in chemical physics, volume 136 of *Advances in Chemical Physics*, 2007, pp. 207–258.

[4] H. Schwertfeger, A. A. Fokin, P. R. Schreiner, Diamonds are a chemist's best friend: Diamondoid chemistry beyond adamantane, Angew. Chem. Int. 47 (2008) 1022–1036. doi:{10.1002/anie.200701684}.

[5] S. Stauss, K. Terashima, Diamondoids: Synthesis, Properties, and Applications, PAN Stanford Publishing, 2017.

[6] W. C. Saslaw, J. E. Gaustad, Interstellar dust and diamonds, Nature 221 (1969) 160. doi:10.1038/221160b0.

[7] R. S. Lewis, T. Ming, J. F. Wacker, E. Steel, interstellar diamonds in meteotites, Nature 326 (1987) 160–162. doi:10.1038/326160a0.

[8] A. P. Jones, L. B. D'Hendecourt, S.-Y. Sheu, H.-C. Chang, C.-L. Cheng, H. G. M. Hill, Surface CH stretch features on meteoric nanodiamonds, Astronom. Astrophys. 416 (2004) 235–241. doi:10.1051/0004-6361:20031708.

[9] H.-C. Chang, J.-C. Lin, J.-Y. Wu, K.-H. Chen, Infrared spectroscopy and vibrational relaxation of CHx and CDx stretches on synthetic diamond nanocrystal surfaces, J. Phys. Chem. 99 (1995) 11081–11088. doi:10.1021/j100028a007.

[10] S.-Y. Sheu, I.-P. Lee, Y. T. Lee, H.-C. Chang, Laboratory investigation of hydrogenated diamond surfaces: implication for the formation and size of interstellar nanodiamonds, Astrophys. J. 581 (2002) L55–L58. doi:10.1086/345519.

[11] O. Guillois, G. Ledoux, C. Reynaud, Diamond Infrared emission bands in circumstellar media, Astrophys. J. 521 (1999) L133–L136. doi:10.1086/312199.

[12] J. Oomens, N. Polfer, O. Pirali, Y. Ueno, R. Maboudian, P. W. May, J. Filik, J. E. Dahl, S. Liu, R. M. K. Carlson, Infrared spectroscopic investigation of higher diamondoids, J. Mol. Spectrosc. 238 (2006) 158–167. doi:10.1016/j.jms.2006.05.001.

[13] O. Pirali, M. Vervloet, J. E. Dahl, R. M. K. Carlson, A. G. G. M. Tielens, J. Oomens, Infrared spectroscopy of diamondoid molecules: New insights into the presence of nanodiamonds in the interstellar medium, Astrophys. J. 661 (2007) 919–925. doi:10.1086/516731.

[14] J. E. Dahl, S. G. Liu, R. M. K. Carlson, Isolation and structure of higher diamondoids, nanometer-sized diamond molecules, Science 299 (2003) 96. doi:10.1126/science.1078239.

[15] P. V. R. Schleyer, A simple preparation of adamantane, J. Am. Chem. Soc. 79 (1957) 3292. doi:10.1021/ja01569a086.

[16] D. Fărcaşiu, H. Bohm, P. V. R. Schleyer, Stepwise elaboration of diamondoid hydrocarbons. synthesis of diamantane from adamantane, J. Org. Chem. 42 (1977) 96–102. doi:10.1021/jo00421a018.

[17] F. Hollowood, M. McKervey, R. Hamilton, J. Rooney, Synthesis of Triamantane, J. of Org. Chem. 45 (1980) 4954–4958. doi:{10.1021/jo01312a026}.

[18] J. E. P. Dahl, J. M. Moldowan, Z. Wei, P. A. Lipton, P. Denisevich, R. Gat, S. Liu, P. R. Schreiner, R. M. K. Carlson, Synthesis of higher diamondoids and implications for their formation in petroleum, Angewandte Chemie International Edition 49 (2010) 9881–9885. doi:https://doi.org/10.1002/anie.201004276.

[19] C. W. Bauschlicher, Jr., Y. Liu, A. Ricca, A. L. Mattioda, L. J. Allamandola, Electronic and vibrational spectroscopy of diamondoids and the interstellar infrared bands between 3.35 and 3.55 µm, Astrophys. J. 671 (2007) 458–469. doi:10.1086/522683.

[20] L. Landt, K. Klünder, J. E. Dahl, R. M. K. Carlson, T. Möller, C. Bostedt, Optical Response of Diamond Nanocrystals as a Function of Particle Size, Shape, and Symmetry, Phys. Rev. Lett. 103 (2009) 047402. doi:10.1103/PhysRevLett.103.047402.

[21] N. Polfer, B. Sartakov, J. Oomens, The infrared spectrum of the adamantyl cation, Chem. Phys. Lett. 400 (2004) 201–205. doi:{10.1016/j.cplett.2004.10.108}.

[22] O. Pirali, H. A. Galue, J. E. Dahl, R. M. K. Carlson, J. Oomens, Infrared spectra and structures of diamantyl and triamantyl carbocations, Int. J. Mass Spectrom. 297 (2010) 55–62. doi:{10.1016/j.ijms.2010.05.018}.

[23] O. Pirali, V. Boudon, J. Oomens, M. Vervloet, Rotationally resolved infrared spectroscopy of adamantane, J. Chem. Phys 136 (2012). doi:{10.1063/1.3666853}.

[24] O. Pirali, V. Boudon, N. Carrasco, E. Dartois, Rotationally resolved IR spectroscopy of hexamethylenete-

tramine (HMT) $C_6N_4H_{12}$, Astronom. Astrophys. 561 (2014). doi:{10.1051/0004-6361/201322660}.

[25] O. Pirali, V. Boudon, Synchrotron-based Fourier transform spectra of the ν_{23} and ν_{24} IR bands of hexamethylenetetramine $C_6N_4H_{12}$, J. Mol. Spectrosc. 315 (2015) 37–40. doi:{10.1016/j.jms.2015.02.004}.

[26] B. Spaun, P. B. Changala, D. Patterson, B. J. Bjork, O. H. Heckl, J. M. Doyle, J. Ye, Continuous probing of cold complex molecules with infrared frequency comb spectroscopy, Nature 533 (2016) 517. doi:{10.1038/nature17440}.

[27] B. A. McGuire, A. M. Burkhardt, S. Kalenskii, C. N. Shingledecker, A. J. Remijan, E. Herbst, M. C. McCarthy, Detection of the aromatic molecule benzonitrile (c−C_6H_5CN) in the interstellar medium, Science 359 (2018) 202–205. doi:{10.1126/science.aao4890}.

[28] A. Burkhardt, R. Loomis, C. Shingledecker, K. L. K. Lee, A. Remijan, M. McCarthy, B. McGuire, Ubiquitous aromatic carbon chemistry at the earliest stages of star formation, Nat. Astron. (2021) 1–7. doi:10.1038/s41550-020-01253-4.

[29] M. McCarthy, K. L. K. Lee, R. Loomis, A. Burkhardt, C. Shingledecker, S. Charnley, M. Cordiner, E. Herbst, S. Kalenskii, E. Willis, C. Xue, A. Remijan, B. McGuire, Interstellar detection of the highly polar five-membered ring cyanocyclopentadiene, Nat. Astron. (2020) 1–5. doi:10.1038/s41550-020-01213-y.

[30] R. Loomis, A. Burkhardt, C. Shingledecker, S. Charnley, M. Cordiner, E. Herbst, S. Kalenskii, K. L. K. Lee, E. Willis, C. Xue, A. Remijan, M. McCarthy, B. McGuire, An investigation of spectral line stacking techniques and application to the detection of $HC_{11}N$, Nature (2021) 188–196. doi:10.1038/s41550-020-01261-4.

[31] D. Chadwick, A. Legon, D. Millen, Microwave-spectra and strcutures of 1-cyano-Adamantane and 1-iodo-Adamantane, J. Chem. Soc., Faraday Trans. 2 68 (1972) 2064–2069. doi:{10.1039/f29726802064}.

[32] M. A. Martin-Drumel, O. Pirali, C. Falvo, P. Parneix, A. Gamboa, F. Calvo, P. Brechignac, Low-energy vibrational spectra of flexible diphenyl molecules: biphenyl, diphenylmethane, bibenzyl and 2-, 3-and 4-phenyltoluene, Phys. Chem. Chem. Phys. 16 (2014) 22062–22072. doi:{10.1039/c4cp03278k}.

[33] O. Pirali, M. Goubet, V. Boudon, L. D'Accolti, C. Fusco, C. Annese, Characterization of isolated 1-aza-adamantan-4-one ($C_9H_{13}NO$) from microwave, millimeter-wave and infrared spectroscopy supported by electronic structure calculations, J. Mol. Spectrosc. 338 (2017) 6–14. doi:10.1016/j.jms.2017.04.020.

[34] M. J. Frisch, G. W. Trucks, H. B. Schlegel, G. E. Scuseria, M. A. Robb, J. R. Cheeseman, G. Scalmani, V. Barone, B. Mennucci, G. A. Petersson, H. Nakatsuji, M. Caricato, X. Li, H. P. Hratchian, A. F. Izmaylov, J. Bloino, G. Zheng, J. L. Sonnenberg, M. Hada, M. Ehara, K. Toyota, R. Fukuda, J. Hasegawa, M. Ishida, T. Nakajima, Y. Honda, O. Kitao, H. Nakai, T. Vreven, J. A. Montgomery, Jr., J. E. Peralta, F. Ogliaro, M. Bearpark, J. J. Heyd, E. Brothers, K. N. Kudin, V. N. Staroverov, R. Kobayashi, J. Normand, K. Raghavachari, A. Rendell, J. C. Burant, S. S. Iyengar, J. Tomasi, M. Cossi, N. Rega, J. M. Millam, M. Klene, J. E. Knox, J. B. Cross, V. Bakken, C. Adamo, J. Jaramillo, R. Gomperts, R. E. Stratmann, O. Yazyev, A. J. Austin, R. Cammi, C. Pomelli, J. W. Ochterski, R. L. Martin, K. Morokuma, V. G. Zakrzewski, G. A. Voth, P. Salvador, J. J. Dannenberg, S. Dapprich, A. D. Daniels, O. Farkas, J. B. Foresman, J. V. Ortiz, J. Cioslowski, D. J. Fox, Gaussian 09 Revision B.01, 2009. Gaussian Inc. Wallingford CT 2009.

[35] T. H. Dunning, Gaussian basis sets for use in correlated molecular calculations .1. The atoms boron through neon and hydrogen, J. Chem. Phys. 90 (1989) 1007–1023. doi:10.1063/1.456153.

[36] W. Gordy, R. Cook, Microwave Molecular Spectra, Wiley Interscience Pub., 1970.

[37] C. M. Western, PGOPHER: A program for simulating rotational, vibrational and electronic spectra, J. Quant. Spectrosc. Radiat. Transf. 186 (2017) 221–242. doi:{10.1016/j.jqsrt.2016.04.010}.

[38] NIST Computational Chemistry Comparison and Benchmark Database, 2020. URL: http://cccbdb.nist.gov/.

[39] H. M. Pickett, The fitting and prediction of vibration-rotation spectra with spin interactions, J. Mol. Spectrosc. 148 (1991) 371–377. doi:{10.1016/0022-2852(91)90393-0}.

[40] W. Lodyga, M. Kreglewski, P. Pracna, S. Urban, Advanced graphical software for assignments of transitions in rovibrational spectra, J. Mol. Spectrosc. 243 (2007) 182–188. doi:{10.1016/j.jms.2007.02.004}.

Supporting information

Rotational and vibrational spectroscopy of 1-cyanoadamantane and 1-isocyanoadamantane

Olivia Chitarra[a,*], Marie-Aline Martin-Drumel[a], Zachary Buchanan[b], Olivier Pirali[a,c]

[a] *Université Paris-Saclay, CNRS, Institut des Sciences Moléculaires d'Orsay, 91405 Orsay, France*
[b] *Department of Chemistry, The University of California Davis, Davis, CA, USA*
[c] *SOLEIL Synchrotron, AILES beamline, l'Orme des Merisiers, Saint-Aubin, 91190 Gif-sur-Yvette, France*

List of Tables

[*] olivia.chitarra@universite-paris-saclay.fr

Table S1: Optimized equilibrium structure for AdaCN

27
AdaCN - MP2/cc-pVTZ

C	0.449098	0.000000	1.449593
H	0.831417	0.881570	1.969707
H	0.831417	-0.881571	1.969707
C	0.966513	0.000000	0.000000
C	-1.080354	0.000000	1.444101
H	-1.437748	-0.000001	2.475862
C	-1.588106	1.250027	0.721704
H	-1.243003	2.148366	1.240361
H	-2.680894	1.267054	0.731534
C	0.449098	1.255385	-0.724796
H	0.831417	1.265031	-1.748316
H	0.831417	2.146602	-0.221390
C	-1.080354	1.250628	-0.722050
H	-1.437748	2.144160	-1.237930
C	-1.588106	0.000000	-1.443407
H	-2.680894	0.000000	-1.463068
H	-1.243003	0.000001	-2.480720
C	0.449098	-1.255384	-0.724797
H	0.831417	-2.146601	-0.221392
H	0.831417	-1.265030	-1.748316
C	-1.588106	-1.250027	0.721703
H	-1.243003	-2.148367	1.240359
H	-2.680894	-1.267054	0.731534
C	-1.080354	-1.250628	-0.722051
H	-1.437748	-2.144159	-1.237932
C	2.425124	0.000000	0.000000
N	3.597827	0.000000	0.000000

Table S2: Optimized equilibrium structure for AdaNC

```
27
AdaNC - MP2/cc-pVTZ
 C                     0.975874    0.000000    0.000000
 C                    -1.058573    0.000000    1.444282
 C                    -1.058573    1.250785   -0.722141
 C                    -1.058573   -1.250785   -0.722141
 C                     0.471517    0.000000    1.446219
 C                     0.471517    1.252463   -0.723110
 C                     0.471517   -1.252463   -0.723110
 C                    -1.566548    1.250165    0.721783
 C                    -1.566548   -1.250165    0.721783
 C                    -1.566548    0.000000   -1.443566
 H                    -1.414656    0.000000    2.476221
 H                    -1.414656    2.144470   -1.238110
 H                    -1.414656   -2.144470   -1.238110
 H                     0.860323   -0.882558    1.959148
 H                     0.860323    0.882558    1.959148
 H                     0.860323    2.137951   -0.215256
 H                     0.860323    1.255393   -1.743892
 H                     0.860323   -1.255393   -1.743892
 H                     0.860323   -2.137951   -0.215256
 H                    -1.221800    2.148475    1.240423
 H                    -2.659184    1.266602    0.731273
 H                    -1.221800   -2.148475    1.240423
 H                    -2.659184   -1.266602    0.731273
 H                    -1.221800    0.000000   -2.480845
 H                    -2.659184    0.000000   -1.462546
 N                     2.400837    0.000000    0.000000
 C                     3.584089    0.000000    0.000000
```